Available online at www.sciencedirect.com
SCIENCE DIRECT®
Catalysis Communications 6 (2005) 582–585
CATALYSIS COMMUNICATIONS
www.elsevier.com/locate/catcom

An alternative way of reporting on the redox behaviour of ceria-based catalytic materials: Temperature–chemical environment–oxidation state diagrams

S. Bernal *, G. Blanco, J.M. Pintado, J.M. Rodríguez-Izquierdo, M.P. Yeste

Departamento de Ciencia de los Materiales e Ingeniería Metalúrgica y Química Inorgánica, Facultad de Ciencias, Universidad de Cádiz, Apartado 40, E-11510 Puerto Real (Cádiz), Spain

Received 20 March 2005; accepted 18 May 2005
Available online 6 July 2005

Abstract

Temperature–chemical environment–oxidation state diagrams are proposed as an alternative way of reporting on the redox behaviour of ceria-based catalytic materials. In these diagrams, the changes occurred in the reduction degree of the investigated materials are plotted against temperature for different chemical atmospheres (5%O_2/He, He, 5%H_2/Ar, and 5%CO/He). Compared to more conventional parameters like oxygen storage capacity, these diagrams allow us to gain a much wider view of the redox response of the investigated system. As an example, the diagrams are used to discuss the redox properties of two different ceria-terbia mixed oxide samples.

1. Introduction

As deduced from some recent monographs [1,2], ceria and ceria-based mixed oxides are being intensively investigated. A major reason for this interest is the relevance of their catalytic applications, in most of cases closely related to their ability for exchanging oxygen with their chemical environment [3–7].

A variety of techniques has been applied to the redox characterisation of these materials [8–10]. Among them, oxygen storage capacity (OSC) is one of the most commonly used [10]. Complete (OSCC), also referred to as ultimate or total, and dynamic (OSCD) oxygen storage capacity measurements are usually distinguished [10,11]. OSCC estimates the top limit amount of oxygen exchanged by the material under certain pre-established conditions [12,13]; OSCD being aimed at evaluating the most readily available oxygen species [10,14–16]. The so-called oxygen buffering capacity (OBC) technique [17–19] may also be included in the OSCD category. OBC, in effect, allows us to quantitatively measure the capability of a redox material to attenuate the oxygen partial pressure oscillations occurring in a gaseous stream. These oscillations are induced by fast pulsing of O_2 over flowing He. Compared to the typical OSCD techniques, in which CO [6,7,10] or H_2 [11,15,16] are used as reducing agents; in the case of OBC experiments, the reducing conditions are created by an inert gas atmosphere [17].

The experimental conditions under which the OSC values are determined, however, are far from standardisation [15]. Key experimental variables like the nature and partial pressure of the reducing agent, or the reduction time and temperature, often differ from one laboratory to the other, thus very much complicating the correlation of OSC values from different sources.

* Corresponding author. Tel.: +34 956 01 63 38; fax: +34 956 01 62 88.
E-mail address: serafin.bernal@uca.es (S. Bernal).
URL: http://www2.uca.es/dept/cmat_qinor/catalisis/grupo.htm (S. Bernal).

1566-7367/$ - see front matter © 2005 Elsevier B.V. All rights reserved.
doi:10.1016/j.catcom.2005.05.011

Moreover, secondary processes other than that implicitly assumed to be involved in the oxidising part of the OSC cycle, i.e. titration of oxygen vacancies, may significantly contribute to the OSC values. Such is the case of hydrogen spillover, which has been shown to play a key role in determining the high OSCD values recorded, even at room temperature, on a $Pt/Ce_{0.68}Zr_{0.32}O_2$ catalyst [15].

This work reports on an alternative way of depicting the redox properties of these materials. By following this approach, a rather broad picture of the redox response of a certain material under a wide range of experimental conditions (temperature and chemical environment) may be summarised in a single plot. As shown in this work, these temperature–chemical environment–oxidation state diagrams constitute an easily readable way of providing much, very useful, information about the investigated systems.

2. Experimental

In this work, two different ceria-terbia mixed oxides: $Ce_{0.80}Tb_{0.20}O_{2-x}$ and $Ce_{0.90}Tb_{0.10}O_{2-y}$, hereafter referred to as CT-80/20 and CT-90/10, respectively, will be studied. They were prepared by co-precipitation with ammonia from an aqueous solution containing the appropriate molar ratio of $Ce(NO_3)_3$ and $Tb(NO_3)_3$. The precipitates were repeatedly washed with distilled water, dried in air at 383 K, and calcined at 873 K, for 4 h. To stabilise the surface area of the resulting oxides, they were reduced under flowing H_2, at 1223 K, for 4 h, then flushed with He at 1223 K, for 1 h, cooled under flowing He to room temperature, and finally re-oxidised by heating them in a flow of 5%O_2/He up to 873 K, 1 h, and cooled under the same atmosphere to 298 K. The BET surface area of the resulting oxide samples was found to be the same: 4 $m^2\ g^{-1}$. Prior to all the experiments, the samples were heated in a flow of 5%O_2/He up to 873 K, then, they were kept for 1 h at this temperature, and finally, they were slowly cooled to 398 K, always under flowing 5%O_2/He. At this temperature, the gas flow was switched to He and the oxides were cooled down to 298 K. By applying this pre-treatment, a reproducible starting redox state for the oxides could be achieved. The experimental protocol applied in this work may be summarised as follows: 200 mg of the oxide samples pre-treated as indicated above, were heated step by step at increasing temperatures from 573 up to 1223 K in flow of either 5%O_2/He, He, 5%H_2/Ar, or 5%CO/He. The gas flow was always 60 $cm^3\ min^{-1}$, and the heating rate: 10 K min^{-1}. The sample was maintained at each of the pre-established temperatures until an apparent redox equilibrium was reached. Then, the heating program started again and a new step was recorded. The redox changes undergone by the sample throughout the whole experiment (Heating ramp and isothermal part of the step) were continuously monitored by analysing the gas flow downstream the reactor. For experiments carried out under flowing He, 5%H_2/Ar, or 5%CO/He, the analytical device consisted of a quadrupole mass spectrometer (MS). For runs performed in a flow of 5%O_2/He, a thermal conductivity detector (TCD) ought to be used, because of the low sensitivity of the MS device to the changes occurred in the chemical composition of gaseous stream. The redox state of the oxide samples was tracked by analysing, respectively, O_2 (*m*/*e*: 32), in the case of experiments performed under flowing 5%O_2/He, and He; H_2O (*m*/*e*: 18) for those run in a flow of 5%H_2/Ar, and CO_2 (*m*/*e*: 44) when the chemically active atmosphere consisted of 5%CO/He. In the latter case, secondary reactions other than the oxygen vacancy creation process were checked not to contribute to the CO_2 formation significantly. The quantitative calibrations were performed by using well characterized oxide samples: a terbium oxide [20], for oxygen, an aged-in-air lanthanum oxide [21], for CO_2, and copper (II) oxide for H_2O. The reference quantitative data were obtained from parallel TG experiments.

3. Results and discussion

3.1. Temperature–chemical environment–oxidation state diagrams

The Ce-Tb mixed oxides pre-treated under the oxidising conditions reported in Section 2 are better described as partly reduced fluorite phases, $Ce_nTb_{1-n}O_{2-x}$. In these oxygen deficient samples, cerium mainly consists of Ce^{4+} species, whereas a significant concentration of both Tb^{3+} and Tb^{4+} ions coexist [22,23]. Since the experiments to be reported below induce a progressive reduction of the investigated oxides, they will lead to phases which may be formulated as $Ce_nTb_{1-n}O_{(2-x)-\delta}$.

As an example, Fig. 1 summarises the results obtained in one of the stepwise reduction experiments carried out on the CT-80/20 mixed oxide sample. In particular, it corresponds to its thermal evolution under flowing He. Upon integration of the oxygen traces recorded at each of the steps, Fig. 1(a), the amount of evolved oxygen, and, therefore, the change (δ) occurred in the stoichiometry of the oxide, could be determined. From these results, the corresponding temperature-oxidation state (oxide stoichiometry) plot, under flowing He, could be built up, Fig. 1(b). By following the same procedure under flowing 5%O_2/He, 5%H_2/Ar, and 5%CO/He, similar temperature–oxidation state plots could be depicted for sample CT-80/20, Fig. 2. A rather similar study could also be performed on the CT-90/10 sample, see for a detail Fig. 3(b).

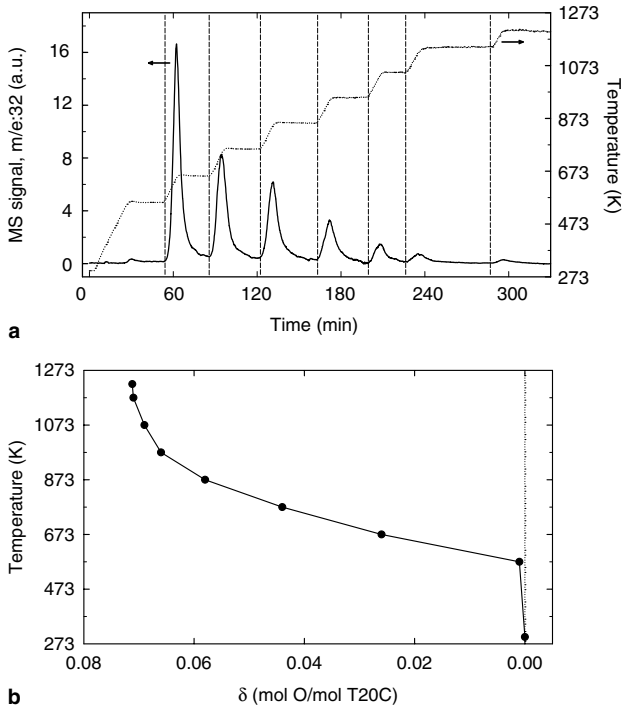

Fig. 1. (a) Stepwise reduction of CT-80/20 under flowing He. (b) Temperature–oxidation state plot as built up from the results reported in (a).

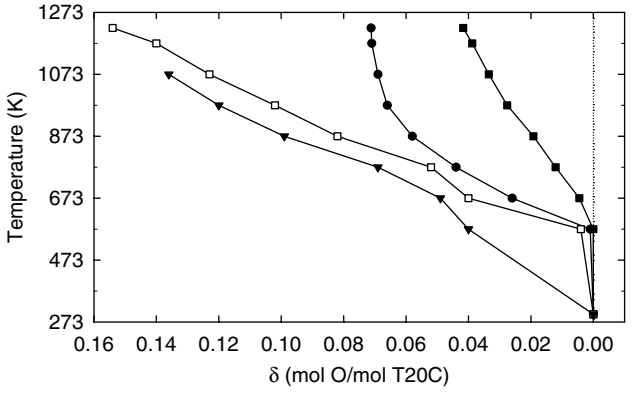

Fig. 2. Temperature–chemical environment–oxidation state diagram corresponding to the CT-80/20 sample. Plots corresponding to the following chemical environments: 5%O_2/He (■); He (●); 5%H_2/Ar (□); and 5%CO/He (▼).

For any of these plots, the successive heating steps imply a progressive reduction of the oxide, the extent of which ($\Delta\delta$) depending on the nature of the flowing gas and the specific temperature step: $Ce_{0.8}Tb_{0.2}O_{(2-x)-\delta 1} \rightarrow Ce_{0.8}Tb_{0.2}O_{(2-x)-\delta 2}$ ($\Delta\delta = \delta_2 - \delta_1$). For all the diagrams in Fig. 2, the common origin in the stoichiometry axis (δ-axis), $\delta = 0$, would correspond to the most oxidised state of the mixed oxide sample, i.e. the state resulting from the application of the standardised pretreatment under flowing 5%O_2/He.

Upon analysing the temperature–chemical environment–oxidation state diagram in Fig. 2, much, very useful, redox information may be drawn from it. Thus, the classic OSCC data, for the different reduction temperatures and flowing gases may be easily deduced from the corresponding $\delta_{i,j}$ values (reduction temperature T_i on the plot recorded under the flowing gas G_j). In addition, the diagram allows us to determine the change occurring in the oxidation state, $\Delta\delta = \delta_{i2,j2} - \delta_{i1,j1}$ ($T_{i2} > T_{i1}$; G_{j2} more reducible environment than that created by G_{j1}), of a certain sample upon varying either the temperature under the same gas flow ($j2 = j1$), the nature of the flowing gas at constant temperature ($i2 = i1$), or both, temperature and chemical environment.

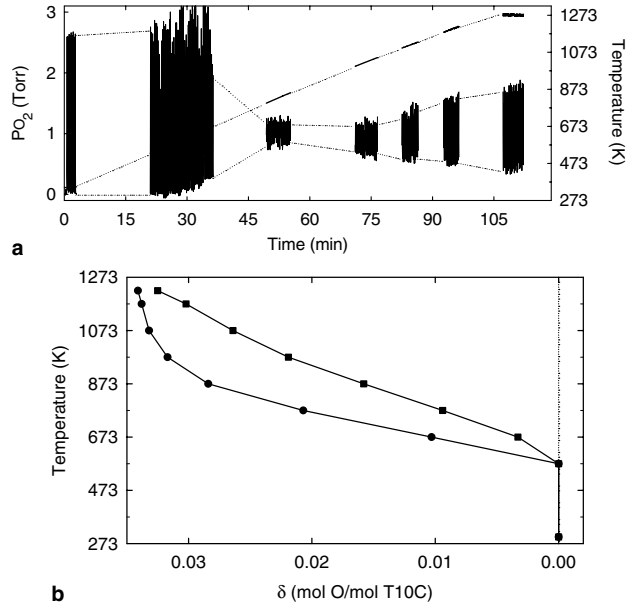

Fig. 3. (a) Temperature-programmed OBC study on the CT-90/10 sample. The experiment consisted of the fast injection 5%O_2/He pulses (pulse frequency 0.1 Hz) over a He stream (He flow: 60 cm^3 min^{-1}), while heating 200 mg of the sample at 10 K min^{-1}. The O_2 signal was recorded with a thermal conductivity detector. (b) Detail of the temperature–chemical environment–oxidation state diagram for this oxide; data corresponding to He (●) and 5%O_2/He (■) chemical environments.

There is some other qualitative information which may be deduced from these diagrams. Thus, the comparison of the low-temperature region, at $T_i = 573$ K, of 5%CO/He, 5%H_2/Ar, He, and 5%O_2/He plots in Fig. 2, strongly suggests that the reduction of the CT-80/20 sample is kinetically controlled under both hydrogen and helium flows, the reduction degree reached by the oxide being much lower than expected from the extrapolation of the results obtained at higher temperatures.

Likewise, the diagrams may help to rationalise some aspects of the redox behaviour of these materials which at a first sight might appear as striking. Thus, Fig. 3 reports on the evolution of the OBC behaviour of the CT-90/10 sample as a function of the temperature. As deduced from this figure, upon increasing the temperature,

the capability of the oxide to attenuate the oscillations in the partial pressure of oxygen goes though a maximum at $T = 873$ K, and then it decreases. If analysed the evolution with T of the He and O_2/He plots in Fig. 3(b), the high-temperature loss of redox efficiency in this sample may reasonably be interpreted as due to thermodynamic reasons, i.e. the progressive decrease of $\Delta\delta = \delta_{i1,j2} - \delta_{i1,j1}$ ($j2$: He; $j1$: 5%O_2/He) upon increasing the temperature above 873 K.

To summarize, by running a rather limited number of simple experiments, the proposed approach allows us to gain a view of the redox behaviour of ceria-based catalytic materials over a wide range of temperatures and chemical environments, thus becoming a useful tool for characterising this sort of materials.

Acknowledgements

Financial support from the MCYT (Project MAT-2002-02782) and the Junta de Andalucía (Grupo FQM-110) is acknowledged

References

[1] A. Trovarelli (Ed.), Catalysis by ceria and related materials, Imperial College Press, London, 2002.
[2] G.A. Adachi, N. Imanaka, Z.C. Kang (Eds.), Binary rare earth oxides, Kluwer Academic Publishers, Amsterdam, 2004.
[3] A. Trovarelli, Catal. Rev. Sci. Eng. 38 (1996) 439.
[4] S. Carrettin, P. Concepción, A. Corma, J.M. López-Nieto, V.F. Puntes, Angew. Chem., Int. Ed. 43 (2004) 2538.
[5] Q. Fu, H. Saltsburg, M. Flytzani-Stephanopoulos, Science 301 (2003) 935.
[6] L. Pino, A. Vita, M. Cordaro, V. Recupero, M.S. Hegde, Appl. Catal. A 243 (2003) 135.
[7] M. Shelef, G.W. Graham, R.W. McCabe, in: A. Trovarelli (Ed.), Catalysis by ceria and related materials, Imperial College Press, London, 2002, p. 343.
[8] S. Bernal, J.J. Calvino, J.M. Gatica, C. López Cartes, J.M. Pintado, in: A. Trovarelli (Ed.), Catalysis by ceria and related materials, Imperial College Press, London, 2002, p. 85.
[9] J.C. Conesa, M. Fernández García, A. Martínez Arias, in: A. Trovarelli (Ed.), Catalysis by ceria and related materials, Imperial College Press, London, 2002, p. 169.
[10] D. Duprez, C. Descorme, in: A. Trovarelli (Ed.), Catalysis by ceria and related materials, Imperial College Press, London, 2002, p. 243.
[11] N. Hickey, P. Fornasiero, J. Kaspar, J.M. Gatica, S. Bernal, J. Catal. 200 (2001) 181.
[12] H. Vidal, J. Kaspar, M. Pijolat, G. Colón, S. Bernal, A. Cordón, V. Perrichon, F. Fally, Appl. Catal. B 27 (2000) 49.
[13] H. Vidal, J. Kaspar, M. Pijolat, G. Colón, S. Bernal, A. Cordón, V. Perrichon, F. Fally, Appl. Catal. B 30 (2001) 75.
[14] M. Boaro, C. de Leitenburg, G. Dolcetti, A. Trovarelli, J. Catal. 193 (2000) 338.
[15] N. Hickey, P. Fornasiero, J. Kaspar, M. Graziani, G. Blanco, S. Bernal, Chem. Commun. (2000) 357.
[16] A. Trovarelli, F. Zamar, J. LLorca, C. de Leitenburg, G. Dolcetti, J.T. Kiss, J. Catal. 169 (1997) 490.
[17] S. Bernal, G. Blanco, M.A. Cauqui, P. Corchado, J.M. Pintado, J.M. Rodríguez-Izquierdo, Chem. Commun. (1997) 1545.
[18] S. Bernal, G. Blanco, M.A. Cauqui, M.P. Corchado, J.M. Pintado, J.M. Rodríguez-Izquierdo, H. Vidal, Stud. Surf. Sci. Catal. 116 (1998) 611.
[19] G. Blanco, J.M. Pintado, S. Bernal, M.A. Cauqui, M.P. Corchado, A. Galtayries, J. Ghijsen, R. Sporken, T. Eickoff, W. Drube, Surf. Interface Anal. 34 (2002) 120.
[20] S. Bernal, G. Blanco, F.J. Botana, J.M. Gatica, J.A. Pérez Omil, J.M. Pintado, J.M. Rodríguez-Izquierdo, P. Maestro, J.J. Braconnier, J. Alloys Comp. 207/208 (1994) 196.
[21] S. Bernal, F.J. Botana, R. García, J.M. Rodríguez-Izquierdo, React. Solids 4 (1987) 23.
[22] J.M. Esteva, R.C. Karnatak, H. Dexpert, M. Gasgnier, P.E. Caro, L. Albert, J. Phys. 47 (1986) C8-955.
[23] H. Arashi, H. Naitoh, M. Ishigame, Solid State Ionics 40/41 (1990) 539.